The following publication Liu, H. and Chan, T.L. (2020), "A coupled LES-Monte Carlo method for simulating aerosol dynamics in a turbulent planar jet", International Journal of Numerical Methods for Heat & Fluid Flow, Vol. 30 No. 2, pp. 855-881 is published by Emerald and is available at https://doi.org/10.1108/HFF-11-2018-0657.

A coupled LES-Monte Carlo method for simulating aerosol dynamics in a turbulent planar jet

Hongmei Liu[1,2,3] and Tat Leung Chan[2,3,#]

[1]School of Mechanical Engineering, Changzhou University, Changzhou, PR China

[2]Department of Mechanical Engineering, The Hong Kong Polytechnic University, Kowloon, Hong Kong

[3]The Hong Kong Polytechnic University, Shenzhen Research Institute, Shenzhen, PR China

[#]Corresponding author

Tat Leung Chan can be contacted at: mmtlchan@polyu.edu.hk

ABSTRACT

Purpose - The purpose of this paper is to study the evolution and growth of aerosol particles in a turbulent planar jet by using the newly developed large eddy simulation (LES)-differentially weighted operator splitting Monte Carlo (DWOSMC) method.

Design/methodology/approach – The DWOSMC method is coupled with LES for the numerical simulation of aerosol dynamics in turbulent flows.

Findings - Firstly, the newly developed and coupled LES-DWOSMC method is verified by the results obtained from a direct numerical simulation-sectional method (DNS-SM) for coagulation occurring in a turbulent planar jet from available literature. Then, the effects of jet temperature and Reynolds number on the evolution of time-averaged mean particle diameter, normalized particle number concentration and particle size distributions (PSDs) are studied numerically on both coagulation and condensation processes. The jet temperature and Reynolds number are shown to be two important parameters that can be used to control the evolution and pattern of PSD in an aerosol reactor.

Originality/value – The coupling between Monte Carlo method and turbulent flow still encounters many technical difficulties. In addition, the relationship between turbulence, particle properties and collision kernels of aerosol dynamics is not yet well understood due to the theoretical limitations and experimental difficulties. In the present study, the developed and coupled LES-DWOSMC method is capable of solving the aerosol dynamics in turbulent flows.

Keywords: Aerosol dynamics, turbulent flow, differentially weighted operator splitting Monte Carlo, jet temperature and Reynolds number, particle size distribution

Article Classification: Research paper

1 Introduction

The phenomenon of aerosol dynamics in turbulent flows is of great interest in a wide range of scientific and industrial applications, for example, air pollutant formation, growth and evolution in the wake of the studied ground vehicle (Chan *et al*., 2010; Chan *et al*., 2019), nanoparticle synthesis in chemical reactive flows (Yu *et al*., 2008; Fang *et al*., 2018), soot particle formation in combustion flames (Celnik *et al*., 2007; Rodrigues *et al*., 2018; Liu *et al.*, 2019), pigment or pharmaceutical additive productions (Stark and Pratsinis, 2002; Dinneen, Deravi *et al*., 2018). In industrial areas, the particle size distributions (PSDs) of aerosol particles affect the properties of the productions while the PSDs of aerosol particles have great influence on the climate change and human health in atmospheric areas. Therefore, population balance modeling subject to turbulent flows plays a significant role in those mentioned areas and applications.

The PSD of aerosols in turbulent flows is affected by several dynamic processes, such as nucleation, coagulation, surface growth (condensation), etc., as well as the convective and diffusion effects of surrounding fluid flows. The general dynamic equation (GDE) is usually used to describe the evolution of aerosol particles (Friedlander, 2000):

$$\frac{\partial n}{\partial t}+\nabla\cdot n\vec{u}=\nabla\cdot D\nabla n+\left[\frac{\partial n}{\partial t}\right]_{\mathrm{nucl}}+\left[\frac{\partial n}{\partial t}\right]_{\mathrm{coag}}+\left[\frac{\partial n}{\partial t}\right]_{\mathrm{cond}} \tag{1}$$

where n is the number density of the particles, $\vec{u}$ is the fluid velocity, D is the diffusion coefficient. The last three terms in the right side of Eq. (1) denote the change on particle number concentration due to the processes of nucleation, coagulation and condensation, respectively.

Great efforts have been made to solve the GDE. Three typical numerical methods arise remarkably due to their excellent computational performance. These methods include the sectional method (SM) (Prakash, *et al.*, 2003; Chen *et al.*, 2015; Rodrigues *et al.*, 2018), the method of moment (MOM) (McGraw, 1997; Chan *et al.*, 2010; Chan *et al.*, 2019), and the Monte Carlo (MC) method (Smith and Matsoukas, 1998; Zhou and He, 2014; Liu and Chan, 2017a & 2017b; 2018a & 2018b; Liu *et al.*, 2019). The SM and MOM are both deterministic methods: the SM is relatively accurate and takes moderate computation time while the MOM is relatively computationally time saving. But they both have disadvantages, for example, the SM usually leads to complicated algorithms and the MOM usually encounters closure problem. In addition, the movement trajectories and

internal structure information of particles cannot be captured by using deterministic methods. The MC method is a stochastic method by using simulated particles to imitate the dynamic behaviors and movement trajectories of aerosols. One disadvantage of MC methods relates to its high computation time requirements. However, with the rapid development of computer technologies, the computation time and memory consumption of MC methods are no longer a major concern. MC method becomes more and more popular because of its stochastic nature and the trajectory and history information of particles can be traced in MC simulations.

In the numerical simulation process of MC method, it needs to track every particle. However, it is impossible to track all the billions of physical particles in real aerosol systems. Therefore, simulated particles are used to represent a certain amount of real physical particles. Every simulated particle can be considered as a representative sample of real particles with the same associated properties, such as density, species, velocity, size, etc., i.e., each simulated particle is weighted by a proper number (Boyd, 1996).

Several different concepts exist on how to choose the weighting scheme and carry out the effect of weighting. Rjasanow and Wagner (1996), Eibeck and Wagner (2001) and Liu and Chan (2017b) used the simulated particles with varying mass weights where they are assigned with a certain mass of real particles. Deville *et al*. (2011) presented the mathematical formalism of the weighted flow algorithms (WFA) and studied how different weighting functions are appropriate for measuring different observables. Patterson *et al*. (2011) and Lee *et al*. (2015) presented a class of fragmentation weight transfer functions to ensure that the number of simulated particles kept constant during fragmentation events and they showed better numerical performance over existing methods. Kotalczyk and Kruis (2017; 2018) and Zhao *et al*. (2010) used the concept of subsystem, every simulated particle represents a certain number of real particles (i.e., every simulated particle has a number-weight). In the present study, the "weight", w_i is defined as the ratio of the number of real particles over the number of simulated particles in Zhao *et al.* (2005; 2010):

$$w_i = \frac{N_r(v)}{N_s(v)} \tag{2}$$

where $N_r(v)$ denotes the number of real particles of volume size, v and $N_s(v)$ denotes the number of simulated particles representing these real particles, $N_r(v)$.

Zhao *et al.* (2005) firstly introduced a multi-Monte Carlo method based on the idea of

"weighted fictitious particle" and later further developed a differentially weighted Monte Carlo (DWMC) method (Zhao *et al.*, 2010) for the numerical simulation of aerosol coagulation. Zhao and Zheng (2013) investigated the spatiotemporal evolution of particle size distributions considering the spatial inhomogeneity of particles using coupled CFD and Monte Carlo method which presented the advantages of Monte Carlo methods. In their study, the differentially weighted Monte Carlo was firstly coupled into CFD to study the interactions of aerosol particles and hydrodynamics. However, only limiting case where coarse particles with high-inertia are considered but the influence of fluid on the particles is not considered. Thus, further development of this method is needed for real aerosol applications. Based on the DWMC method, Liu and Chan (2016; 2018a; 2018b) firstly developed a differentially weighted operator splitting Monte Carlo (DWOSMC) method that uses the operator splitting technique to efficiently couple the differentially weighted Monte Carlo (DWMC) method with the deterministic methods to simulate complex aerosol dynamic behaviors.

From Eq. (1), it can be seen that the surrounding fluid flows can induce the spatial inhomogeneity of particle distributions and have great impacts on the dynamic processes and PSD of aerosols. Therefore, the coupling of the fluid and particles should be considered. Indeed, a lot of research works have been done in inhomogeneous aerosol systems. Rigopoulos (2007) solved the closure problem of the source term of population balance equation (PBE) by a Lagrangian particle method-based probability density function (PDF) approach. He applied this method in a partially stirred aerosol reactor to study the significance of the interactions of turbulence with chemistry-particle formation mechanisms. Hao *et al*. (2013) simulated the process of titania nanoparticle synthesis by considering the effects of nucleation, agglomeration and sintering by a fast PBE-Monte Carlo method. Zhou and He (2014) and Zhou *et al*. (2014) investigated the formation and evolution of aerosols in turbulent mixing layer using both DNS and Monte Carlo methods. Köhn *et al*. (2018) have recently presented a 3D particle Monte Carlo method to study the nucleation of sulphuric acid molecules.

Considering the coupling between the particle dynamics and turbulent flows, there are three common methods for the calculation of multiphase flows, namely direct numerical simulation (DNS), Reynolds-averaged Navier-Stokes (RANS) and large eddy simulation (LES), respectively. LES is quite a powerful tool for the numerical simulation of turbulent flows and is quite popular because it acquires a moderate computational cost for obtaining

the spatial-temporal evolution of the coherent turbulent flow structures. Chan *et al.* (2010) coupled the aerosol dynamics with LES to study the exhaust particle formation and evolution in the wake of the studied ground vehicle. Sung *et al.* (2011) used a multiscale computational model based on the LES to study nanoparticle formation and evolution in a turbulent flame reactor. Pesmazoglou *et al.* (2016; 2017) used a multi-collision Monte Carlo method in which one simulated particle may collide with several simulated particles simultaneously. They successfully coupled this algorithm into gas flows to study the particle aggregation in a turbulent jet using LES approach.

In the present study, the developed DWOSMC method (Liu and Chan, 2018a; 2018b) are newly coupled into CFD to study the aerosol dynamics in turbulent flows where large eddy simulation (LES) is used to calculate the fluid flow field. Turbulent jet flows have a wide range of applications and have attracted interests from many researchers (Chan, *et al.*, 2008; Zhou and Chan, 2011; Pesmazoglou *et al.*,2017). They have conducted numerous studies on the evolution and growth of aerosol particles in turbulent jets accounting for different kinds of aerosol dynamic behaviors (Chan *et al.*, 2006; Lin *et al.*, 2007; Chan *et al.*, 2018). Hence, a turbulent planar jet flow is also studied in the present study. Firstly, the developed and coupled LES-DWOSMC method is verified by the results obtained from a direct numerical simulation-sectional method (DNS-SM) (Miller and Garrick, 2004) for coagulation occurring in a turbulent planar jet. Then the effects of jet temperature and Reynolds number on the evolution of time-averaged mean particle diameter, normalized particle number concentration and normalized particle size distributions (PSDs). The jet temperature and Reynolds number prove to be two important parameters that can be used to control the evolution and pattern of PSD in an aerosol reactor.

2 Numerical methodology

2.1 Eulerian equations for the continuous gas phase

The transport of the continuous fluid phase is governed by the well-known Navier-Stokes (N-S) equations which describe the conservation of mass, momentum and energy. Large eddy simulation (LES) provides an appropriate compromise between the computational precision and efficiency. In LES, the turbulent flows are decomposed into two parts of large- and small-scale structures: the large eddies are directly computed on a Eulerian

grid, while the small eddies are modelled (Chan *et al.*, 2008). In LES, the filtered N–S Equation is written as,

$$\frac{\partial \rho}{\partial t}+\frac{\partial(\rho \bar{u}_i)}{\partial x_i}=0 \tag{3}$$

$$\frac{\partial(\rho \bar{u}_i)}{\partial t}+\frac{\partial(\rho \bar{u}_i \bar{u}_j)}{\partial x_j}=-\frac{\partial \bar{p}}{\partial x_i}+\frac{\partial}{\partial x_j}(\mu \frac{\partial \bar{u}_i}{\partial x_j})-\frac{\partial \tau_{ij}}{\partial x_j} \tag{4}$$

where u_i is the velocity, p is the pressure, ρ is the density and μ is the viscosity. τ_{ij} refers to the subgrid scale (SGS) stress tensor, representing the motions at scales that are smaller than the filter width; τ_{ij} is written as,

$$\tau_{ij}=\rho(\overline{u_i u_j}-\bar{u}_i \bar{u}_j) \tag{5}$$

τ_{ij} cannot be solved explicitly, therefore modelling is required. One method is the eddy viscosity modelling.

$$\tau_{ij}-\frac{1}{3}\delta_{ij}\tau_{ii}=-2\nu_t \bar{S}_{ij} \tag{6}$$

where ν_t is subgrid viscosity coefficient, and $\bar{s}_{ij}$ is the filtered rate-of-strain tensor.

$$\bar{S}_{ij}=\frac{1}{2}\left(\frac{\partial \bar{u}_j}{\partial x_i}+\frac{\partial \bar{u}_i}{\partial x_j}\right) \tag{7}$$

For solving the subgrid viscosity coefficient, the SGS model of Smagorinsky (1963) is often used in the studies because of its simplicity and lower computation time and memory consumption.

In Smagorinsky model, the subgrid viscosity coefficient, ν_t is expressed as:

$$\nu_t = (C_s\Delta)^2|\bar{S}_{ij}| \tag{8}$$

where $|\bar{S}_{ij}| = \sqrt{2\bar{S}_{ij}\bar{S}_{ij}}$, C_s is the Smagorinsky coefficient, Δ is the cube root of the local grid volume and is used as the representative length scale of SGS turbulence with the Smagorinsky coefficient.

2.2 Lagrangian Particle Tracking

The dispersed particle phase is described by a Lagrangian Monte Carlo method, and the governing equation of the position and velocity of a particle is given by the Newton's second law (Fan *et al.*, 1997; Sommerfeld, 2001):

$$\frac{\mathrm{d}x_{p,i}}{\mathrm{d}t} = u_{p,i} \tag{9}$$

$$\frac{\mathrm{d}u_{p,i}}{\mathrm{d}t} = \frac{3}{4}\frac{\rho}{\rho_p d_p} c_\mathrm{D} (u_i - u_{p,i})|\vec{u} - \vec{u_p}| + f_s \tag{10}$$

where $x_{p,i}$ is the position, $u_{p,i}$ is the velocity of the particles, u_i is the velocity of the continuous gas phase and d_p is the diameter of the dispersed particles. The first term in the right hand side of Eq. (10) denotes the drag force that the carrier flow imposes on the particles. The drag coefficient, c_D is formulated by,

$$\begin{gathered} c_\mathrm{D} = 24(1+0.15 Re_p^{0.687})/Re_p \text{ when } Re_p < 1000 \qquad \text{and} \\ c_\mathrm{D} = 0.44, \text{ when } Re_p \geq 1000 \end{gathered} \tag{11}$$

where Re_p is the relative Reynolds number,

$$Re_p = \frac{d_p|\vec{u} - \vec{u_p}|}{\nu} \tag{12}$$

In Eq. (10), f_s represents the contributions from forces other than drag force, for example, gravity, lift, Basset, etc. It is observed that the Stokes drag is the dominant force for a large scale of density ratios between the dispersed particles and the carrier gas flows while the effect of other forces imposed on particles is only about 1% (Armenio and Fiorotto, 2013). Therefore, the force considered in the present study is only the drag force.

2.3 The coupled LES-DWOSMC method

In the previous studies of Liu and Chan (2018a; 2018b), a differentially weighted operator splitting Monte Carlo (DWOSMC) method was firstly developed for simulating complex aerosol dynamics. In the present study, the developed DWOSMC method is newly coupled into the Eulerian-Lagrangian model for simulating two-phase flows.

2.3.1 Mathematical modelling

1) The determination of time-step

a) The time-step for the gas phase flow

The time-step for the gas phase flow is limited by the following procedures:

Firstly, the time step size is selected so that the maximum Courant-Friedrichs-Lewy (CFL) number is always less than 0.5.

$$CFL = u\frac{\Delta t_1}{\Delta x} \leq 0.5 \tag{13}$$

Then, it is supposed that coagulation only occurs between particles inside one computational grid (Kruis *et al*., 2012; Zhao and Zheng, 2013; Pesmazoglou *et al*, 2017). Therefore, the displacement of the fluid element in one time-step should not be larger than the length of a computational grid. This time scale is written as,

$$\tau_f = \min(l_i/u_i) \tag{14}$$

where l_i and u_i are the length of grid, i and the fluid average velocity inside the grid, i, respectively.

Lastly, the time-step should also be smaller than the particle relaxation time (Zhao and Zheng, 2013) as,

$$\tau_p = \rho_p d_p^2/(18\rho_f \nu) \tag{15}$$

Therefore, the chosen time-step for the gas phase flow is used as,

$$\Delta t \leq \min(\Delta t_1, \tau_f, \tau_p) \tag{16}$$

b) The time-step for the aerosol dynamics

The time scale for the aerosol dynamics should be smaller than the characteristic time scales for each aerosol dynamic process.

For coagulation events, the characteristic time scale is calculated from Eq. (17):

$$\Delta t_{\text{coag}} = \min|_{\forall i}\left(V_l / \sum_{j=1, j\neq i}^{N_{s,l}} K_{ij}^{'}\right) \tag{17}$$

where V_l and $N_{s,l}$ are the volume of the computational grid, l and the number of simulated particles in the grid, respectively. $K_{ij}^{'}$ is the normalized coagulation kernel considering the weights of particles, i and j:

$$K_{ij}^{'} = 2K_{ij}w_j\max(w_i, w_j)/(w_i + w_j) \tag{18}$$

where K_{ij} is the coagulation kernel.

For condensation process, the characteristic time scale is calculated as:

$$\Delta t_{\text{cond}} = \min|_{\forall i}(v_i/I_0(v)) \tag{19}$$

where v_i denotes the volume of simulated particle, i and $I_0(v)$ denotes the condensation kernel.

Therefore, the used time-step should be smaller than all the mentioned characteristic time scales. The time-step for aerosol dynamics is used as:

$$\delta t \leq \min(\Delta t_{\text{coag}}, \Delta t_{\text{cond}}) \tag{20}$$

2) Treatment of aerosol dynamic processes

a) Coagulation

The change in particle size distribution due to coagulation event is (Wei, 2013),

$$\left[\frac{\partial n}{\partial t}\right]_{\text{coag}} = \frac{1}{2}\int_0^v K(v-\tilde{v},\tilde{v})n(\tilde{v})n(v-\tilde{v})\mathrm{d}\tilde{v} - \int_0^\infty K(v,\tilde{v})n(v)n(\tilde{v})\mathrm{d}\tilde{v} \tag{21}$$

where $K(v,\tilde{v})$ denotes the coagulation kernel that represents the rate of particles with volume, v and particles with volume, $\tilde{v}$ coagulate with each other.

The calculation of coagulation process is based on the DWMC method developed by Zhao *et al.* (2010). The probability of particle, i coagulates with others is written as,

$$P_i = 1-\exp(-V_l C_i \delta t/2) \tag{22}$$

where V_l denotes the volume of the computational grid, l and C_i denotes the coagulation rate of particle, i, and is calculated as:

$$C_i = \frac{1}{V_l^2}\sum_{j=1,j\neq i}^{N_{s,l}} K_{ij}^{'} \tag{23}$$

Particle i is chosen to be the first coagulation particle when a random number is smaller than P_i,

$$r_1 \leq P_i \tag{24}$$

where r_1 is a random number generated from a uniform distribution between 0 and 1.

The coagulation partner of particle, j is selected according to Eq. (25). If Eq. (25) is satisfied, it is assumed that coagulation occurs between particles, i and j. If not, the remaining particles are examined until Eq. (25) is satisfied.

$$r_2 \leq K_{ij}^{'}/\max(K_{mn}^{'})|_{\forall m,\forall n} \tag{25}$$

where r_2 is a random number generated from a uniform distribution between 0 and 1.

After two coagulation particles, i and j are selected, the coagulation process is calculated as Eq. (26). The size, weight, spatial position and velocity field of the particles are updated after the coagulation event (Zhao and Zheng, 2013).

If

$$w_i=w_j,\begin{cases} w_i^{'}=w_i/2;\ v_i^{'}=v_i+v_j;\ x_{p,i}^{'}=x_{p,i};\ u_{p,i}^{'}=(v_iu_{p,i}+v_ju_{p,j})/(v_i+v_j); \\ w_j^{'}=w_j/2;\ v_j^{'}=v_i+v_j;\ x_{p,j}^{'}=x_{p,i};\ \ u_{p,j}^{'}=(v_iu_{p,i}+v_ju_{p,j})/(v_i+v_j); \end{cases} \tag{26a}$$

Or if

$$w_i\neq w_j,\begin{cases} w_i^{'}=\max(w_i,w_j)-\min(w_i,w_j);v_i^{'}=v_m|_{w_m=\max(w_i,w_j)}; \\ x_{p,i}^{'}=x_{p,m}|_{w_m=\max(w_i,w_j)};\ u_{p,i}^{'}=u_{p,m}|_{w_m=\max(w_i,w_j)}\ ; \\ w_j^{'}=\min(w_i,w_j);v_j^{'}=v_i+v_j; \\ x_{p,j}^{'}=x_{p,n}|_{w_n=\min(w_i,w_j)};\ u_{p,j}^{'}=(v_iu_{p,i}+v_ju_{p,j})/(v_i+v_j); \end{cases} \tag{26b}$$

where $w_i^{'}$, $w_j^{'}$, $v_i^{'}$, $v_j^{'}$, $x_i^{'}$, $x_j^{'}$, $u_i^{'}$ and $u_j^{'}$ are the weight, volume, spatial position and velocity of the updated simulated particles, *i* and *j* after the occurrence of coagulation process. In the present study, the density of all particles is uniform and keeps constant. Therefore, the conservation of particle volume in Eq. (26) indicates the conservation of mass, and thus the velocity calculation of the particles can be based on the volume of particles.

b) Condensation.

The condensation process has influence on the size distribution of particles by increasing the particles' volume.

The change in particle size distribution due to condensation process (Ramabhadran *et al*., 1976) is,

$$\left[\frac{\partial n(v,t)}{\partial t}\right]_{\text{cond}}=-\frac{\partial(I_0n)}{\partial v}(v,t) \tag{27}$$

In the present study, the weights of the simulated particles do not change when dealing with the condensation process, thus the total particle number concentration does not vary on account of condensation process while the volume of particle, i will change accordingly,

$$\frac{dv_i}{dt}=I(v) \tag{28}$$

Specifically, the condensation process is calculated within half time-step, $\delta t/2$ in this DWOSMC method as:

$$v_i^{'} = v_i + I(v)\delta t/2 \tag{29}$$

$$w_i^{'} = w_i \tag{30}$$

$$x_{p,i}^{'} = x_{p,i} \tag{31}$$

$$u_{p,i}^{'} = u_{p,i} \tag{32}$$

c) Integration.

The governing equation of aerosol dynamics consists of different physical processes. The splitting methods generally stand out when an operator or equation can be split into several parts that are much easier to solve, and then are composed to form the integrator. Consider a simple time-dependent differential equation, $\mathrm{d}x/\mathrm{d}t = X(x)$, three steps are involved to implement the splitting methods (McLachlan and Quispel, 2002):

i) Selecting a set of vector fields, X_i such that $X = \sum(X_i)$;

ii) Integrating each X_i; and

iii) Combining these solutions to yield an integrator for X.

Then the operator splitting method can be described as:

$$\exp(\triangle tX) = \exp(\triangle tX_1)\exp(\triangle tX_2) + \mathcal{O}(\triangle t^2) \tag{33a}$$

$$= \exp(1/2\triangle tX_2)\exp(\triangle tX_1)\exp(1/2\triangle tX_2) + \mathcal{O}(\triangle t^3) \tag{33b}$$

$$= \exp(1/2\triangle tX_1)\exp(\triangle tX_2)\exp(1/2\triangle tX_1) + \mathcal{O}(\triangle t^3) \tag{33c}$$

where X refers to the total process, X_1 and X_2 refer to two different sub-processes and $\triangle t$ refers to one time-step. Eq. (33a) is of first-order accuracy while Eqs. (33b) and (33c) are of second-order accuracy (Zhou et al., 2014).

In this DWOSMC method, the second-order Strang splitting method is applied for managing stochastic and deterministic aerosol dynamic processes which is expressed as:

$$\exp(\delta tX) = \exp\left(\frac{1}{2}\delta tX_{\mathrm{d}}\right)\exp(\delta tX_{\mathrm{s}})\exp\left(\frac{1}{2}\delta tX_{\mathrm{d}}\right) + \mathcal{O}(\delta t^3) \tag{34}$$

where X_{s} is the coagulation process and X_{d} is the condensation process.

2.3.2 Algorithmic implementation

A brief outline of the algorithm of the developed and coupled LES-DWOSMC method is given as follows:

(a) Initialization. The boundary conditions and initial values of both the gas and particle phases are assigned. For the gas phase, the initial thermal and flow fields (e.g., temperature, pressure, velocity, etc.) are characterized. For the particle phase, the particle properties (e.g., weight, number concentration, size distribution, etc.) are characterized.

(b) Choose a time-step, Δt for the gas phase flow.

(c) Solving the gas flow fields. The physical conservation equations (i.e., mass, momentum and energy) of the continuous gas phase are solved where the flow field properties (i.e., velocity, pressure, temperature, etc.) are obtained.

(d) Updating the spatial position and velocity field of particles. The motion of particles is governed by Eqs. (9) and (10), and thus the particle field can be solved by the Lagrangian particle tracking (LPT) method.

(e) Choose a time-step, δt for the aerosol particles.

(f) Start M (i.e., $M = \Delta t / \delta t$) Monte Carlo loops.

(g) Treatment of particle dynamic processes.

(h) The properties (e.g., weight, number concentration, size distribution, etc.) of simulated particles are updated.

(i) If the current MC loop number, R does not reach the predetermined MC loop number, M, then start a new MC loop. Otherwise, if R is equal to M, quit the Monte Carlo loop for the aerosol particles.

(j) If the calculation time, t is smaller than the predetermined stopping time, t_{stop}, then repeat from steps (b) to (i). Otherwise, if t reaches t_{stop}, the averaged results are calculated to output the status of two-phase flow fields, and particle size and concentration distributions.

The flowchart of the developed and coupled LES-DWOSMC algorithm is shown in Fig. 1.

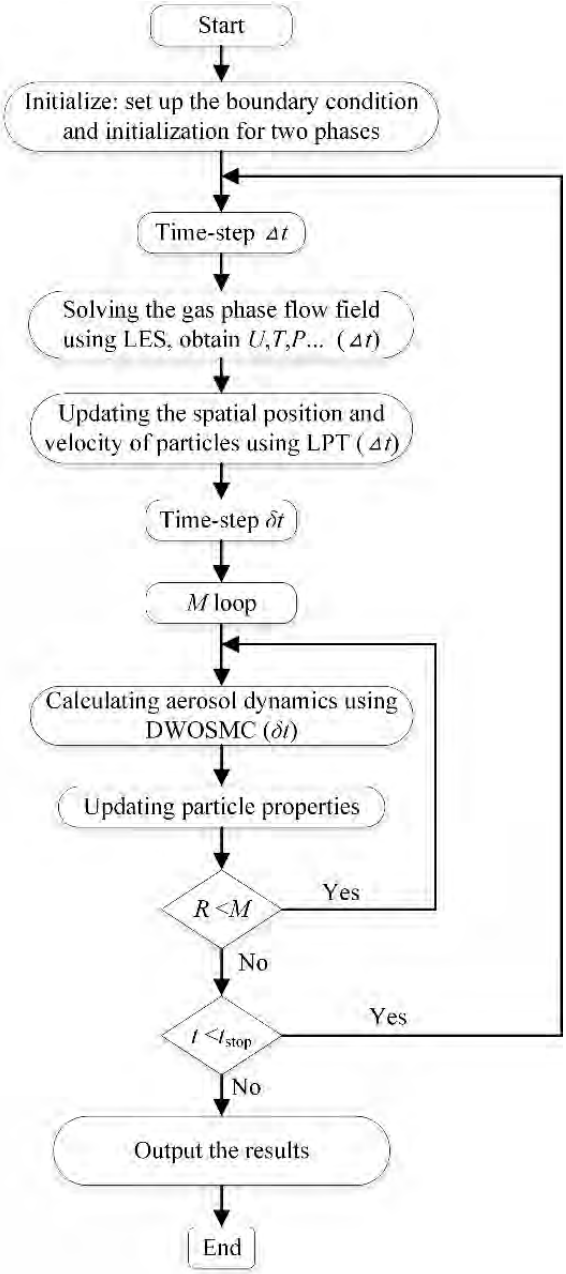

Fig. 1 Flowchart of the developed and coupled LES-DWOSMC algorithm.

2.4 Numerical schemes

The developed DWOSMC is coupled into the LES model to simulate the dynamic behaviors of dispersed aerosol particles. The DWOSMC program is implemented into the OpenFOAM C++ library. OpenFOAM is a desired CFD package because it is open source. A new Eulerian-Lagrangian solver is built by implementing the Lagrangian Particle Tracking (LPT) approach to the existing solver of pimpleFoam. In the present study, the

Smagorinsky eddy-viscosity model is used to solve the unknown sub-grid stresses of the fluid flow field (Smagorinsky, 1963; Pesmazoglou *et al*., 2017), and the Smagorinsky coefficient used is 0.173 (Pesmazoglou *et al*., 2017). Transient computing scheme is used and the convergence criterion for the relative residual of the velocity, continuity and other variables is set as 1×10^{-6} (Chan *et al*., 2018).

3 Results and Discussion

Firstly, the numerical verification and implementation of the newly developed and coupled LES-DWOSMC method are examined on the numerical model used by Miller and Garrick (Miller and Garrick, 2004) by calculating aerosol coagulation in an incompressible and isothermal turbulent planar jet, the results are verified with the direct numerical simulation-sectional method (DNS-SM) (Miller and Garrick, 2004). After the initial verification, this LES-DWOSMC method is used to study the effects of temperature and Reynolds number of a turbulent planar jet on the evolution of aerosol particles under the coagulation and condensation processes.

3.1 Configuration and model description

Fig. 2 shows a planar jet flow configuration examined by Miller and Garrick (Miller and Garrick, 2004) and also used in the present study, where the spatial coordinates, x and y are the stream-wise and cross-stream directions, respectively. The diameter of the planar jet, D is 1 mm, and the computational domain in x and y directions is $12\times7D$. The velocity of the main flow is $U_1 = 95$ m/s, and the co-flow velocity is $U_2 = 0.55U_1$. The Reynolds number of the jet flow based on the jet diameter is, $\mathrm{Re}_D = U_1D/\nu \cong 4000$ (Miller and Garrick, 2004).

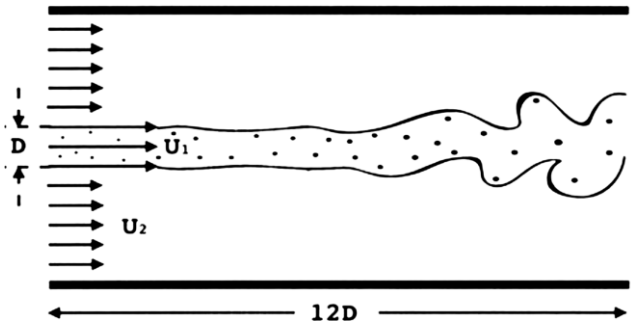

Fig. 2 A sketch map of a planar jet flow (Miller and Garrick, 2004).

Three different grid densities (coarse meshes: 33600 cells, medium meshes: 70200 cells, and fine meshes: 279600 cells) are used to examine the grid independence test in the present study. The velocity distribution profiles at x/D= 6 for different grid density cases are shown in Fig. 3(a). It can be well observed that the velocity distribution profiles calculated from the three studied meshes do not tend to have obvious difference in the present study. Furthermore, the transient distributions of the vorticity in z-direction ($\Omega_z = \partial v/\partial x - \partial u/\partial y$) calculated from the three studied meshes are shown in Fig. 3(b) to (d). The results show that the vortex shedding starts at around x/D = 6 in Fig. 3(b) and at around x/D = 3.5 in both Fig. 3(c) to (d) which are consistent with the findings of Miller and Garrick (2004). Since the coherent vortex structure of fluid gas has a large effect on the particle dispersion pattern, the grid density with 70200 cells is proved to be sufficient to describe the gas flow in the present study and is selected to perform the present numerical simulations in consideration of both computational accuracy and efficiency.

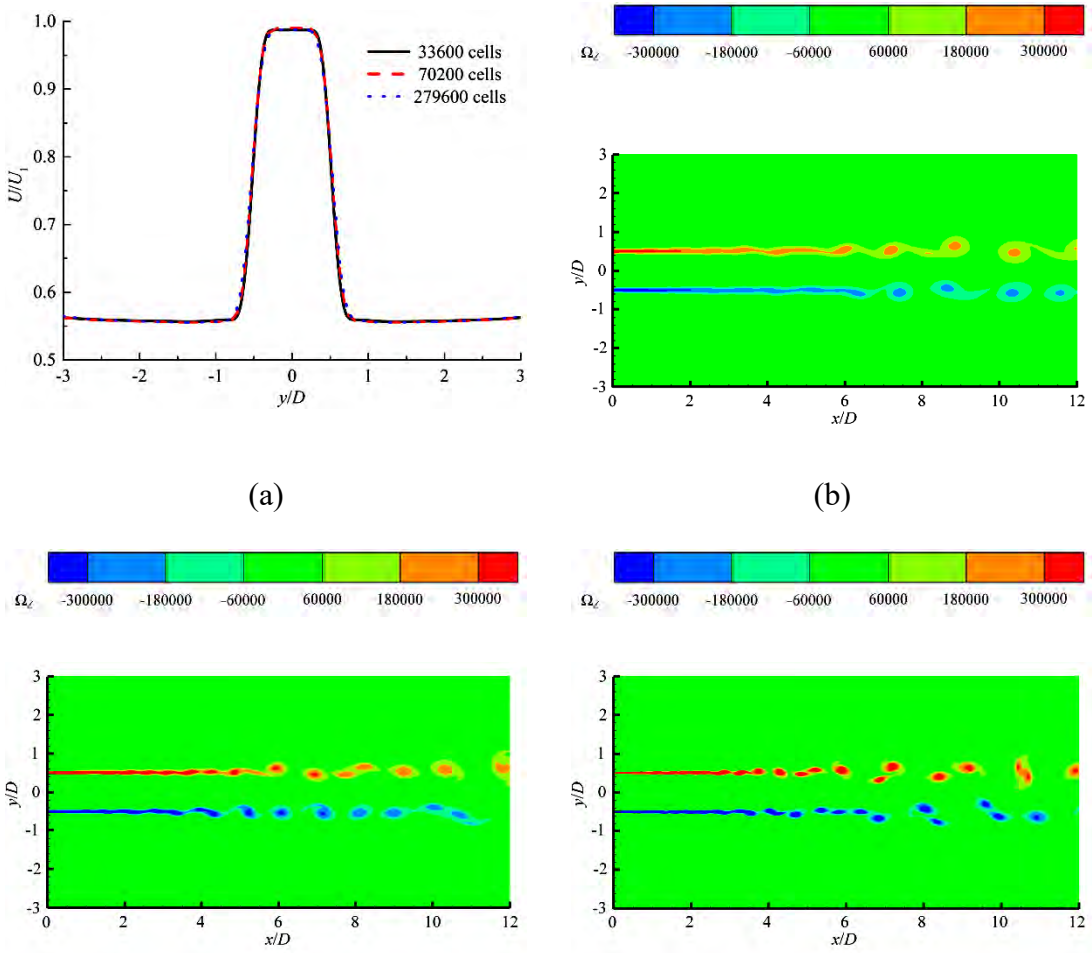

(c) (d)

Fig. 3 Effect of different grid densities on (a) the velocity distribution profiles, and the transient vorticity distributions for using (b) coarse meshes: 33600 cells, (c) medium meshes: 70200 cells, and (d) fine meshes: 279600 cells.

Since the aerosol dynamics are highly affected by the coherent vortex structure of fluid gas, it is essential to examine the vorticity field. Fig. 4 shows the transient evolution of the vorticity in z-direction at four non-dimensional times (i.e., $t^* = tU_1/D$ = 3.8, 9.5, 15.2 and 28.5) with Re_D = 4000 and T_j =300 K according to the time for the stream-wise flows to reach x/D = 2, 6, 10 and after the flow is stable. Vorticity is generated at the interface of two parallel streams where the jet and the co-flow mix together. Vortex shedding starts at around x/D = 3.5 and the peak value of vorticity magnitude becomes smaller along the stream-wise direction, which is in accordance with the findings of Miller and Garrick (2004).

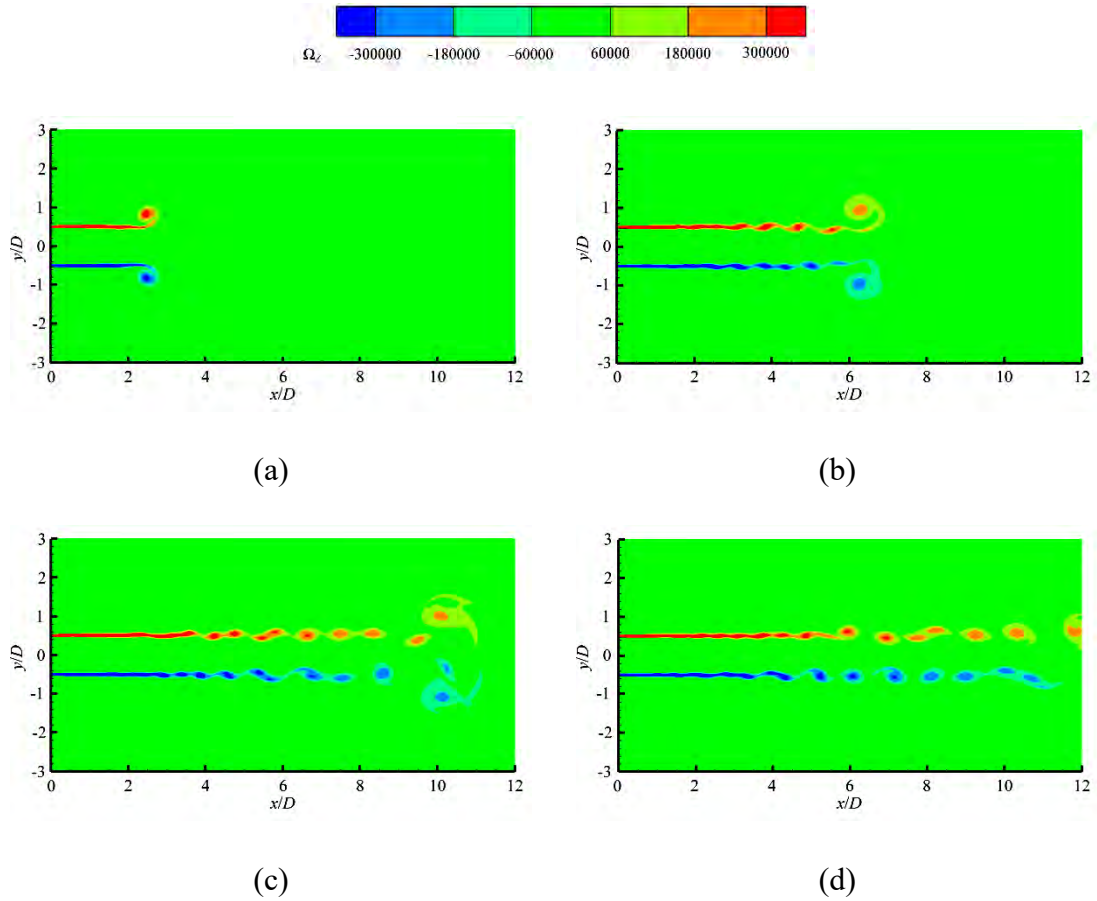

(a) (b)

(c) (d)

Fig. 4 Contours of the transient evolution of vorticity at (a) t^* = 3.8, (b) t^* = 9.5, (c) t^* = 15.2 and (d) t^* = 28.5 with Re_D = 4000 and T_j =300 K.

The simulated results of time-averaged stream-wise velocity of the gas phase flow at four different axial positions (i.e., x/D=2, 6, 10, 11.5) from LES are compared with the results obtained from direct numerical simulation (DNS) (Miller and Garrick, 2004). The velocity distribution profiles are shown in Fig. 5. It can be seen that the mean velocity distributions obtained from LES agree well with those obtained from DNS, and the selected computational grid density is deemed adequate in the present study.

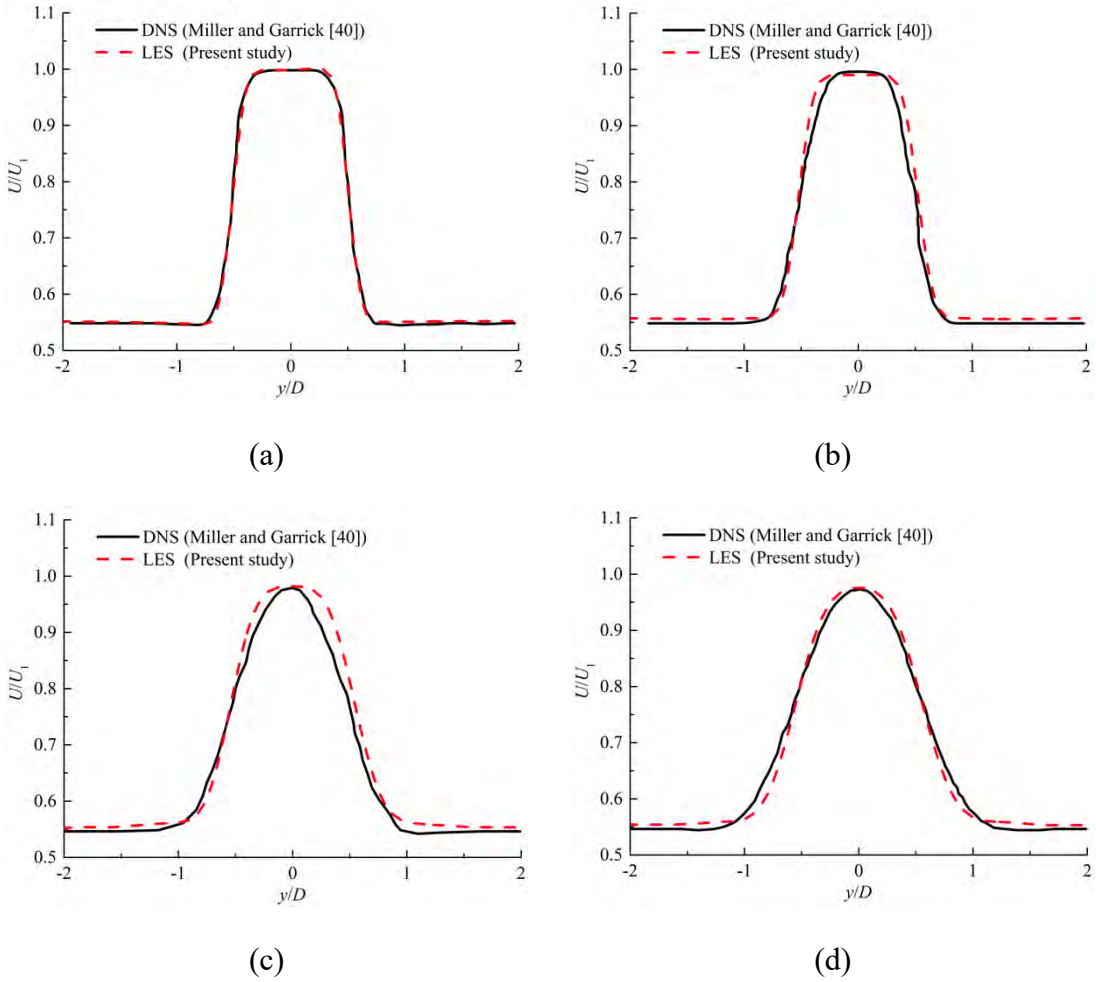

Fig. 5 The planar jet velocity distribution profiles obtained from LES and DNS (Miller and Garrick, 2004) at (a) x/D = 2, (b) x/D = 6, (c) x/D = 10 and (d) x/D = 11.5 with Re_D = 4000 and T_j = 300 K.

3.2 Coagulation in turbulent flows

3.2.1 Coagulation in turbulent flows

In the first case studied in the present study, the fluid flow is incompressible and isothermal with both jet and surrounding temperature of 300K. Particles with density of 1800 kg/m^3 are initially uniformly distributed with a diameter of 1 nm and injected with a volume fraction of $\varphi_v \sim \mathcal{O}(1\times10^{-7})$ as similarly used by Miller and Garrick (2004). The initial conditions and simulated parameters for aerosol dynamics in turbulent flows are summarized in Table 1. The coagulation rate under free molecule regime given by Eq. (35) is considered.

$$K(v,\tilde{v}) = (\frac{6}{\pi})^{2/3}(\frac{\pi k_B T}{2\rho_p})^{1/2}(\frac{1}{v}+\frac{1}{\tilde{v}})^{1/2}(v^{1/3}+\tilde{v}^{1/3})^2 \quad (35)$$

Table 1. Simulated parameters for aerosol dynamics in turbulent flows (Miller and Garrick, 2004)

Particle density (kg/m^3)	1,800
Particle diameter (nm)	1
Particle volume fraction	1×10^{-7}
Injection velocity of the jet (m/s)	95
Velocity of the co-flow (m/s)	52.25
Temperature of the continuous gas phase (K)	300
The number of simulated particles used	70,000
The number of simulated particles in each grid cell	50
Coagulation model	Eq. (35)
Turbulence model	LES model

The time-averaged mean particle diameters at four different axial positions, *y/D* obtained from the LES-DWOSMC method are compared with the DNS-SM (Miller and Garrick, 2004) and are shown in Fig. 6. It can be seen that the time-averaged mean diameter of the particles becomes larger and the region filled with particles becomes wider along the stream-wise direction. The results obtained from the LES-DWOSMC method are consistent with the results obtained from DNS-SM (Miller and Garrick, 2004). Both

results show that in the interface region of the two parallel streams, the particle diameter tends to be larger than in the jet centreline. It is because particles are affected by the vortex structure in the interface region, and the particles acquire longer residence time to coagulate and form larger particles (Miller and Garrick, 2004; Pesmazoglou and Kempf, 2017). It can be concluded that this LES-DWOSMC method proves to be capable of simulating aerosol coagulations in turbulent flows.

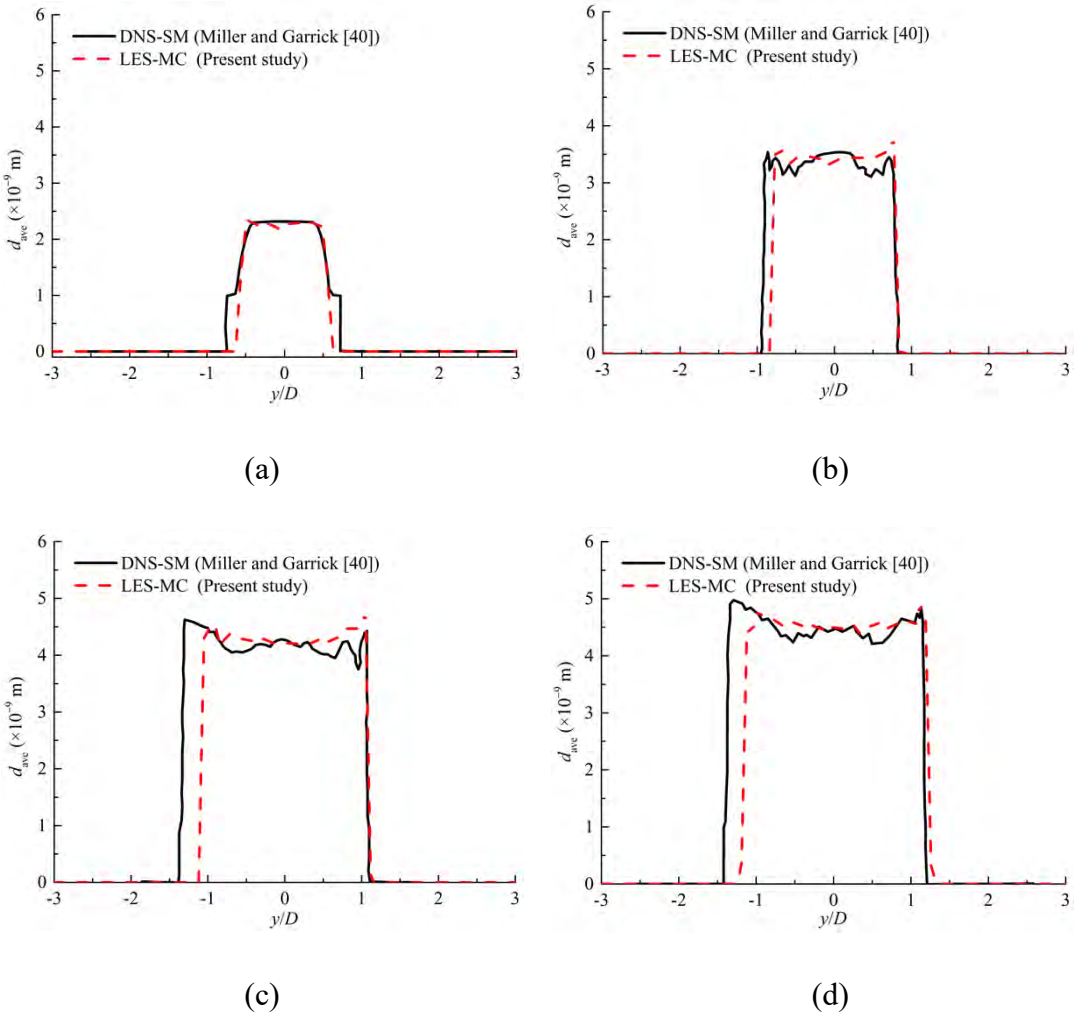

Fig. 6 Time-averaged mean particle diameter obtained from LES-DWOSMC method and DNS-SM (Miller and Garrick, 2004) at (a) x/D =2, (b) x/D = 6, (c) x/D = 10 and (d) x/D = 11.5.

One advantage of Monte Carlo methods over deterministic methods is that the properties (e.g., diameter, volume, location, velocity, etc.) of each simulated particle can be obtained. In the present study, the transient states and dispersion characteristics of the particle field

by using the discrete simulated particles are shown in Fig. 7.

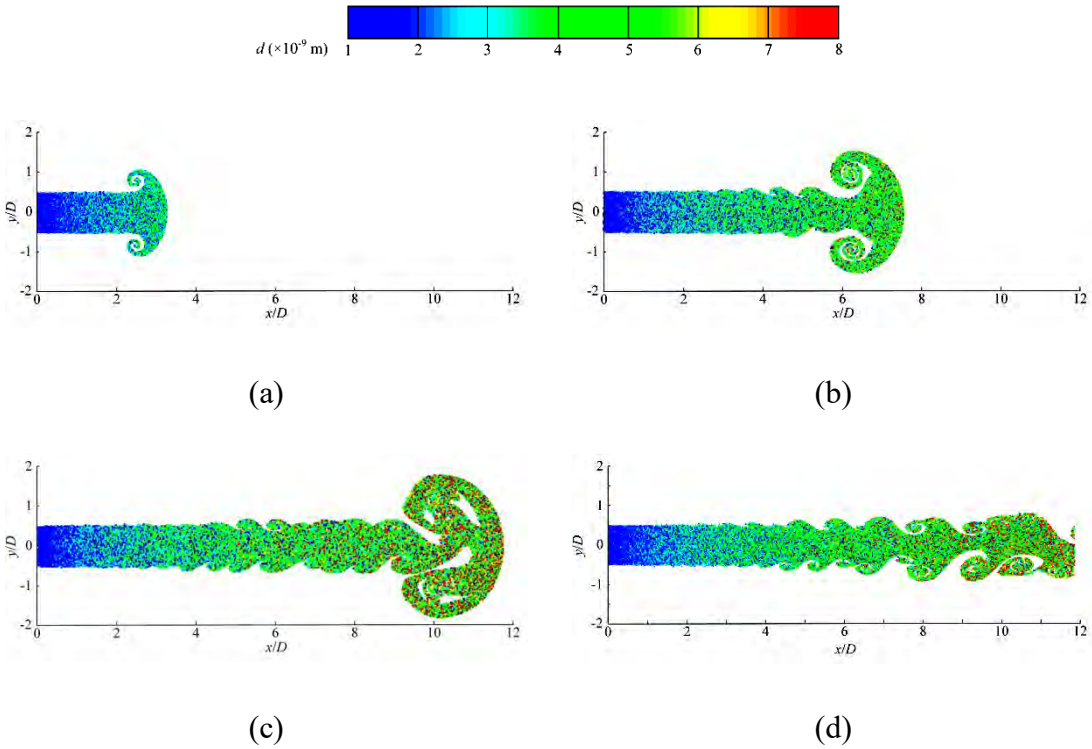

Fig. 7 Transient particle field distribution coloured by the diameter of particles at (a) $t^* = 3.8$, (b) $t^* = 9.5$, (c) $t^* = 15.2$ and (d) $t^* = 28.5$ with $\mathrm{Re}_D = 4000$ and $T_j = 300$ K.

The transient dispersion pattern of the particles is affected by the vortex structure of the fluid flows and the transient distribution of the particles is quite similar to the contours of vorticity shown in Fig. 4. It can also be seen that the diameters of particles increase along the stream-wise direction because coagulation process makes the diameter of particles larger.

In this LES-DWOSMC method, each simulated particle may have different weights. From Eq. (21), it can be seen that the weights of the simulated particles become smaller after the coagulation events. The transient dispersion pattern of the particles colored by their weights at time of $t^* = 28.5$ is shown in Fig. 8. The particles are injected with weights of $\mathcal{O}(\times 10^7)$, with the development of the jet flow, coagulation occurs, the weights of

simulated particles become smaller along the stream-wise direction, x. In the outlet of the jet, the weights of simulated particles are $\mathcal{O}(\times 10^4)$. Since the number of the simulated particles is assumed to be constant in the LES-DWOSMC method, the reduction of weights implies the reduction of the number of real physical particles in the turbulent aerosol system.

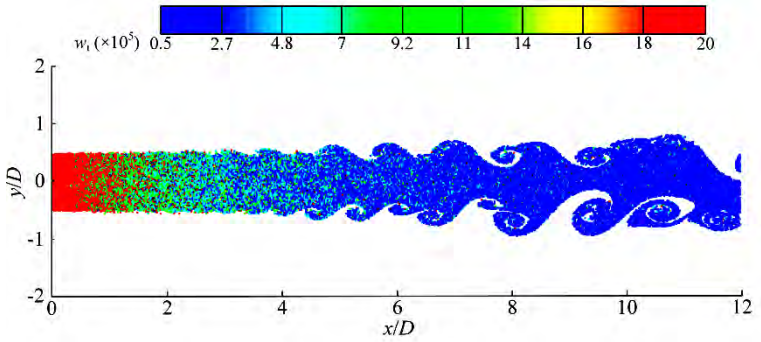

Fig. 8 A typical transient particle field distribution colored by the weights of simulated particles at $t^* = 28.5$, $\mathrm{Re}_D = 4000$ and $T_j = 300$ K.

3.2.2 The effect of temperature on turbulent coagulation

In the processes of soot formation and nanoparticle synthesis, aerosol particles are usually exposed in a very high temperature environment which will affect the aerosol dynamics processes. In the present study, particles are injected for three different jet temperatures, T_j = 300K, 1300K and 2300K, respectively. Other initial conditions of the particles are set up to be the same as those mentioned in Section 3.2.1.

The transient particle dispersion patterns of the three different cases (i.e., T_j = 300K, 1300K and 2300K) at $t^* = 9.5$ and $t^* = 28.5$ with $\mathrm{Re}_D = 4000$ are shown in Fig. 9. With the increase of the jet temperature, the particle dispersion pattern does not change but it is clearly noticed that particles tend to have a larger diameter at the end of the jet flow when the jet temperature is higher. It is because particles become more active with higher jet temperature which will result in more effective coagulation events and thus the particle diameter becomes larger.

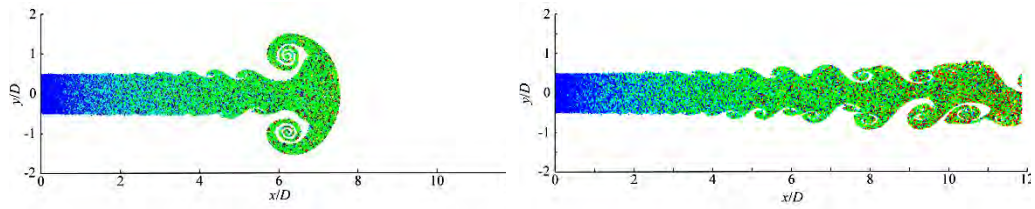

(a) T_j = 300K, t^* = 9.5 (b) T_j = 300K, t^* = 28.5

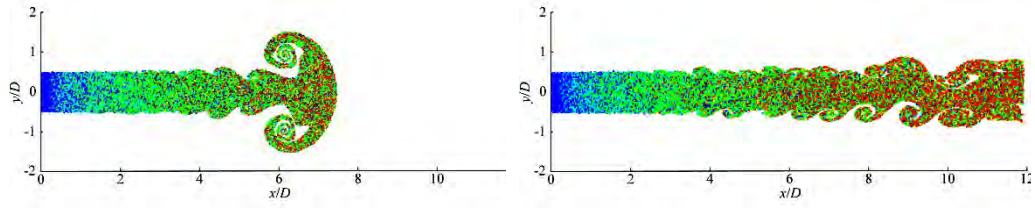

(c) T_j = 1300K, t^* = 9.5 (d) T_j = 1300K, t^* = 28.5

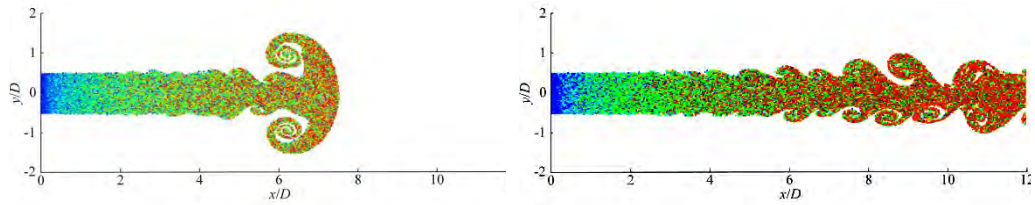

(e) T_j = 2300K, t^* = 9.5 (f) T_j = 2300K, t^* = 28.5

Fig. 9 Transient particle field distributions at Re_D = 4000 for different t^* and T_j.

The evolution of the time-averaged mean particle diameter, d_{ave} and the normalized particle number concentration, $N_c/N_{c,0}$ (where N_c is the particle number concentration and $N_{c,0}$ is the particle number concentration in the jet inlet) at the position of y/D = 0 of the studied cases for different jet temperatures are shown in Fig. 10. It is clearly shown that for each studied case, d_{ave} increases and $N_c/N_{c,0}$ decreases along the stream-wise direction because the coagulation event occurs. With the increase of jet temperature, the mean particle diameter also shows an observable increase and the reduction of particle number concentration becomes faster because the higher temperature can cause more frequent collisions between particles and strengthen the coagulation effects.

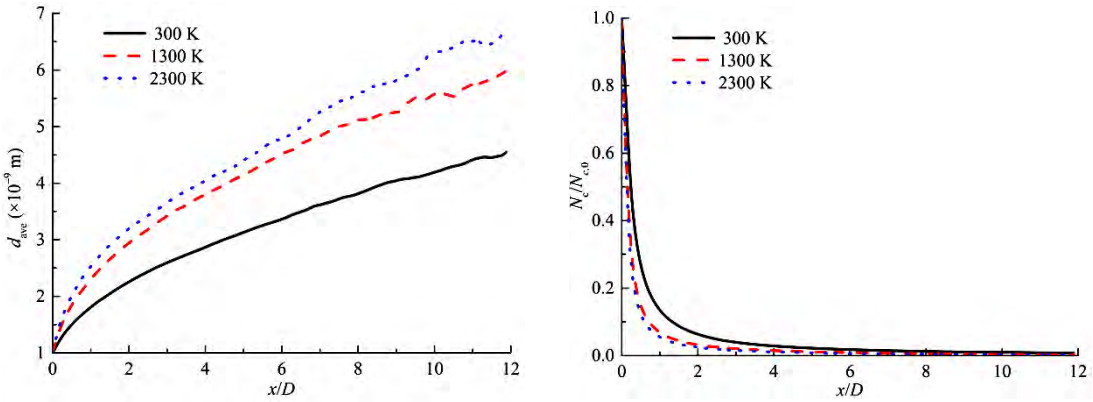

Fig. 10 The spatial evolutions of the time-averaged (a) mean particle diameter, d_{ave} and (b) normalized particle number concentration profiles, $N_c/N_{c,0}$ at $y/D = 0$ and $Re_D = 4000$ for different T_j.

The normalized particle size distributions (PSDs) of the studied cases for three different jet temperatures, T_j are shown in Fig. 11. The peak value of the PSD curve moves towards the larger end of the particle size range and the curve of PSD becomes wider when the axial position, x/D moves along the stream-wise direction. For different studied cases, when the temperature of the jet increases at the same position, the peak value of the PSD curve also moves towards the larger end of the particle size range. The curve of PSD also becomes wider which implies that the coagulation effect is enhanced with the increase of jet temperature. Therefore, it can be concluded that the PSD of aerosol particles or the coagulation effect of the particles can be properly controlled by introducing particles into different environmental temperatures.

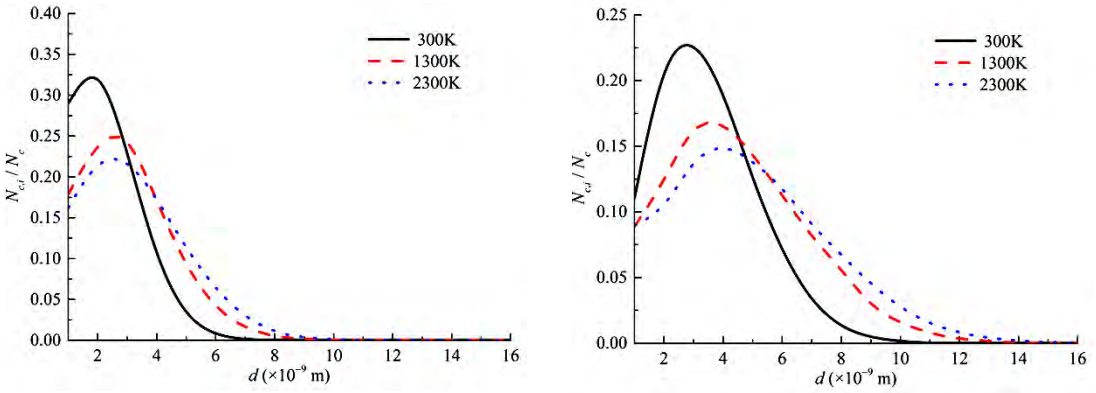

(a) (b)

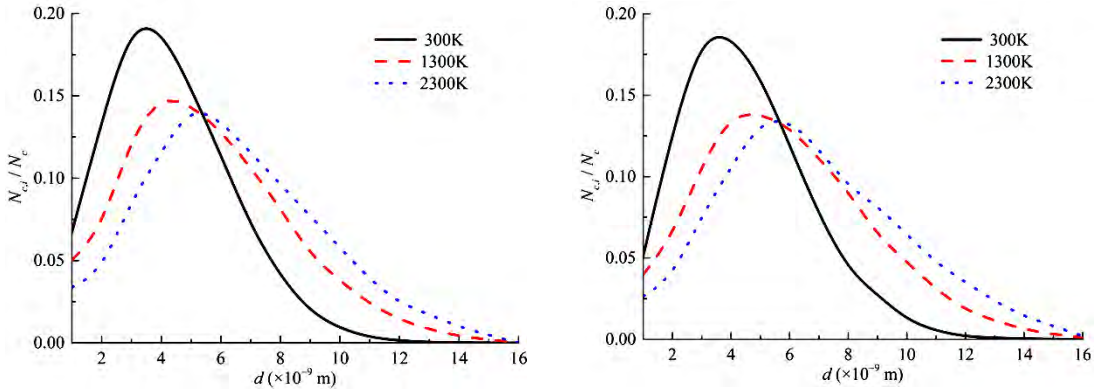

(c) (d)

Fig. 11 PSD profiles at (a) $x/D = 2$, (b) $x/D = 6$, (c) $x/D = 10$ and (d) $x/D = 11.5$ at $y/D = 0$ and $\mathrm{Re}_D = 4000$ for different jet temperatures, T_j.

3.2.3 The effect of Reynolds number on turbulent coagulation

Four corresponding jet Reynolds numbers, $\mathrm{Re}_D = 2000$, 4000, 6000, and 8000 are studied on aerosol coagulation process in the turbulent planar jet for T_j=1300K (as similar evolution tendency can be obtained from different temperature cases, only the case of $T_j = 1300$K is shown here). The evolution of the time-averaged mean particle diameters, d_{ave} and the normalized particle number concentration, $N_c/N_{c,0}$ at the position of $y/D = 0$ for the studied cases are shown in Fig. 12.

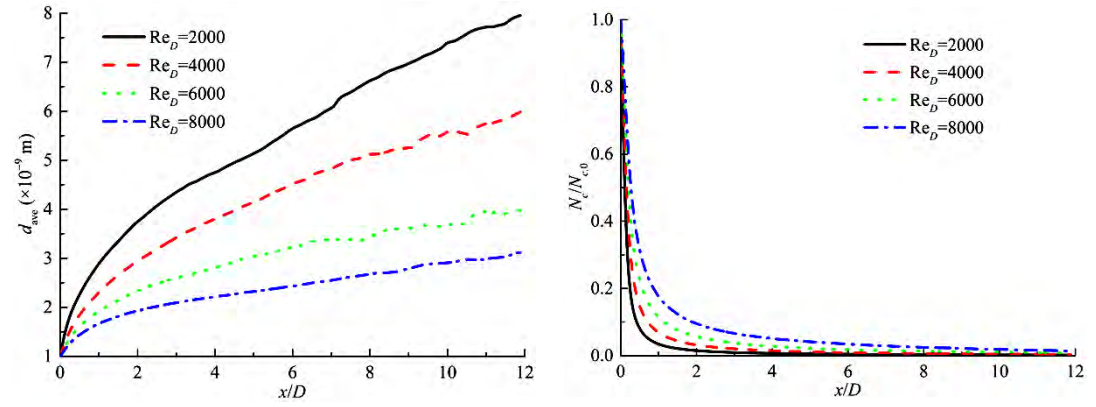

(a) (b)

Fig. 12 The spatial evolutions of the time-averaged (a) d_{ave} and (b) $N_c/N_{c,0}$ profiles at $y/D = 0$ and $T_j = 1300$K for different Re_D.

In Fig. 12, it can be observed that with the increase of Re_D, the mean particle diameter, d_{ave} decreases and the particle number concentration increases which implies that the coagulation process is reduced with the increase of Re_D. It is because with the increase of the velocity of the fluid flow and particles, the residence time of the particles in the flow region decreases, which results in shorter time for the particles to coagulate to form larger particles.

The normalized particle size distributions (PSDs) of different Re_D cases are shown in Fig. 13. It can be seen that the PSD becomes higher and narrower with the increase of Re_D at both positions of $x/h = 2$ and 10. When Re_D reaches 8000, the PSD still evolves observable change from $x/D = 2$ to $x/D = 10$ even though the velocity of the particles is fast and coagulation happens at low probabilities. It can be seen that when $Re_D = 8000$, the PSD at $x/D = 2$ is a drastically decreasing curve at almost the same rate in the whole particle size range while the PSD at $x/D = 10$ has an interval (from $d = 2.5$ to 4.5 nm) where the curve decreases very slowly as shown in Fig. 13. It can also be observed that when $Re_D = 6000$, there are two peaks of the PSD at the position of $x/D = 10$: the two peaks appear at $d = 1$ nm and around 4 nm, respectively. While when $Re_D = 2000$, 4000 and 8000, there is only one peak for the PSD. Furthermore, when $Re_D \leq 6000$ (i.e., $Re_D = 2000$ and 4000), the PSD at $x/D = 10$ firstly increases and then decreases, while when $Re_D \geq 6000$ (i.e., $Re_D = 8000$), the PSD at $x/D = 10$ monotonically decreases. Therefore, the shape and magnitude (i.e., height, width, and the number of peaks) of the PSD can be fully controlled by adjusting the Re_D for the studied cases accordingly where coagulation process occurs in the turbulent planar jet.

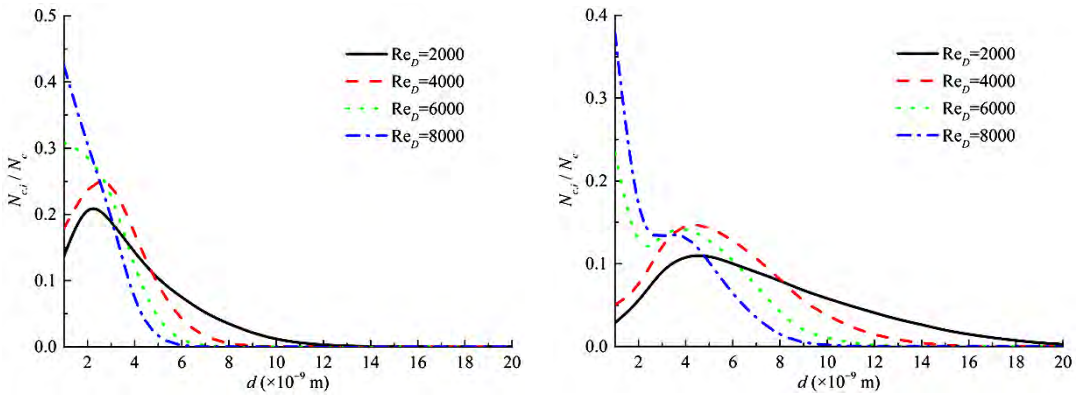

(a) (b)

Fig. 13 PSD profiles at axial positions of (a) $x/D = 2$ and (b) $x/D = 10$ at $y/D = 0$ and $T_j = 1300$K for different Re_D.

3.3 Coagulation and condensation in the turbulent planar jet

3.3.1 The effect of jet temperature on turbulent coagulation and condensation

The effect of jet temperature, T_j on two simultaneous aerosol dynamic processes (i.e., coagulation and condensation) is studied in the turbulent planar jet. The initial conditions and T_j studied are the same as previous cases studied in Section 3.2. The coagulation kernel in free molecule regime is also used and the adopted condensation rate is written as,

$$I(v) = \sigma v \tag{36}$$

where σ is 5×10^3/s.

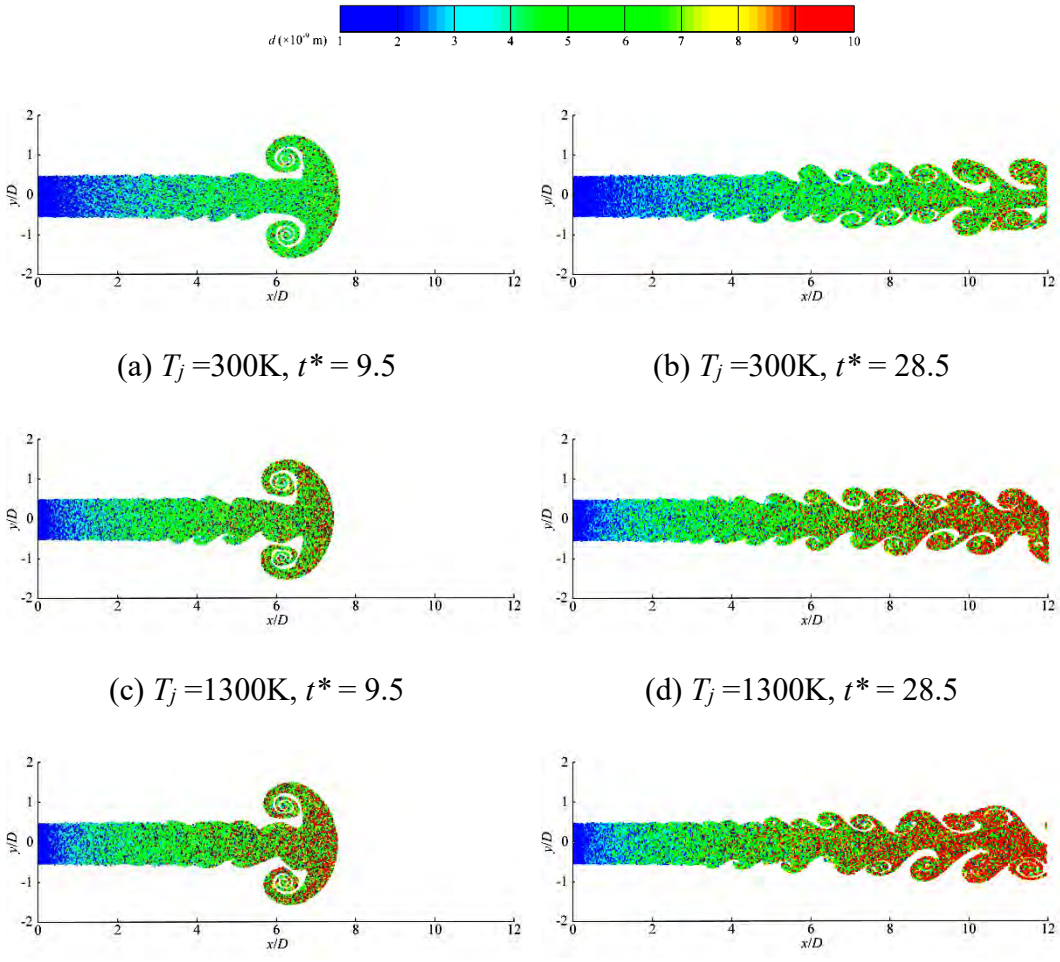

(a) T_j =300K, t^* = 9.5 (b) T_j =300K, t^* = 28.5

(c) T_j =1300K, t^* = 9.5 (d) T_j =1300K, t^* = 28.5

(e) T_j =2300K, t^* = 9.5 (f) T_j =2300K, t^* = 28.5

Fig. 14 Transient particle field distribution of simultaneous coagulation and condensation cases at Re_D =4000 for different T_j and t^*.

The transient particle distributions of different jet temperature cases (i.e., T_j = 300K, 1300K and 2300K) are shown in Fig. 14. The dispersion pattern of the particles does not change while the diameter becomes larger remarkably than the cases as shown in Fig. 9 because the condensation process is a particle growing process but does not change the particle number concentration distribution. It can also be seen that the particle dispersion pattern is mostly determined by the gas flow and the vortex structures in all cases studied.

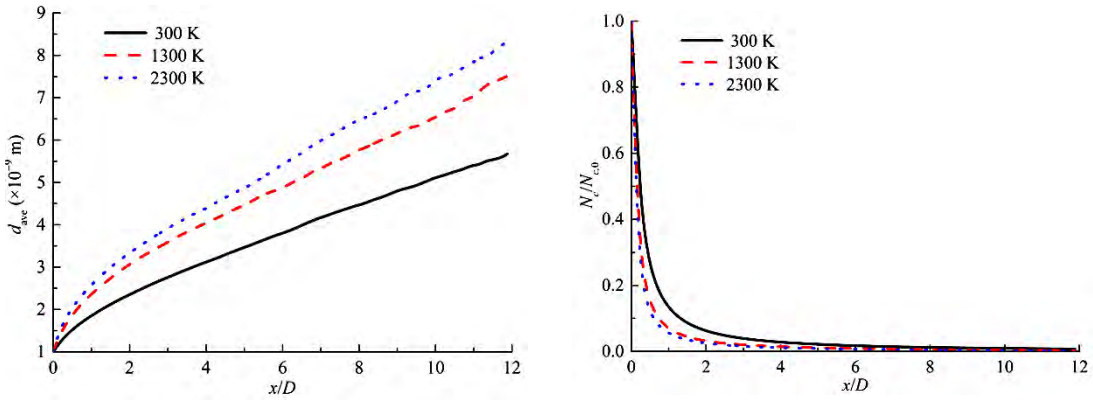

Fig. 15 The spatial evolutions of (a) d_{ave} and (b) $N_c/N_{c,0}$ profiles of simultaneous coagulation and condensation cases at y/D = 0 and Re_D =4000 for different x/D and T_j.

The evolutions of the time-averaged mean particle diameters, d_{ave} and the normalized particle number concentration, $N_c/N_{c,0}$ at y/D = 0 for different T_j are shown in Fig. 15. Compared Fig. 15 with Fig. 10, it can be seen that when coagulation and condensation simultaneously occur, for the same T_j cases, the growth of mean particle diameter is much faster than those cases where only coagulation occurs. The reduction rate of particle number concentration does not significantly change because the occurrence of condensation events does not change the particle number concentration.

The normalized PSDs for different T_j are shown in Fig. 16. Compare Fig. 16 with Fig. 11, the shape of the PSD curves and the evolutions of PSD do not significantly change, while the PSD curve tends to be much wider and the peak value of the PSD curve moves towards the larger end of the particle size range at the same position of x/D of each case studied. This is because the condensation events will result in larger size of particles and therefore affect the PSD. With the increase of T_j, the PSD at the same position of x/D becomes lower and wider, which is the same as the conclusion from the cases studied where only coagulation takes place.

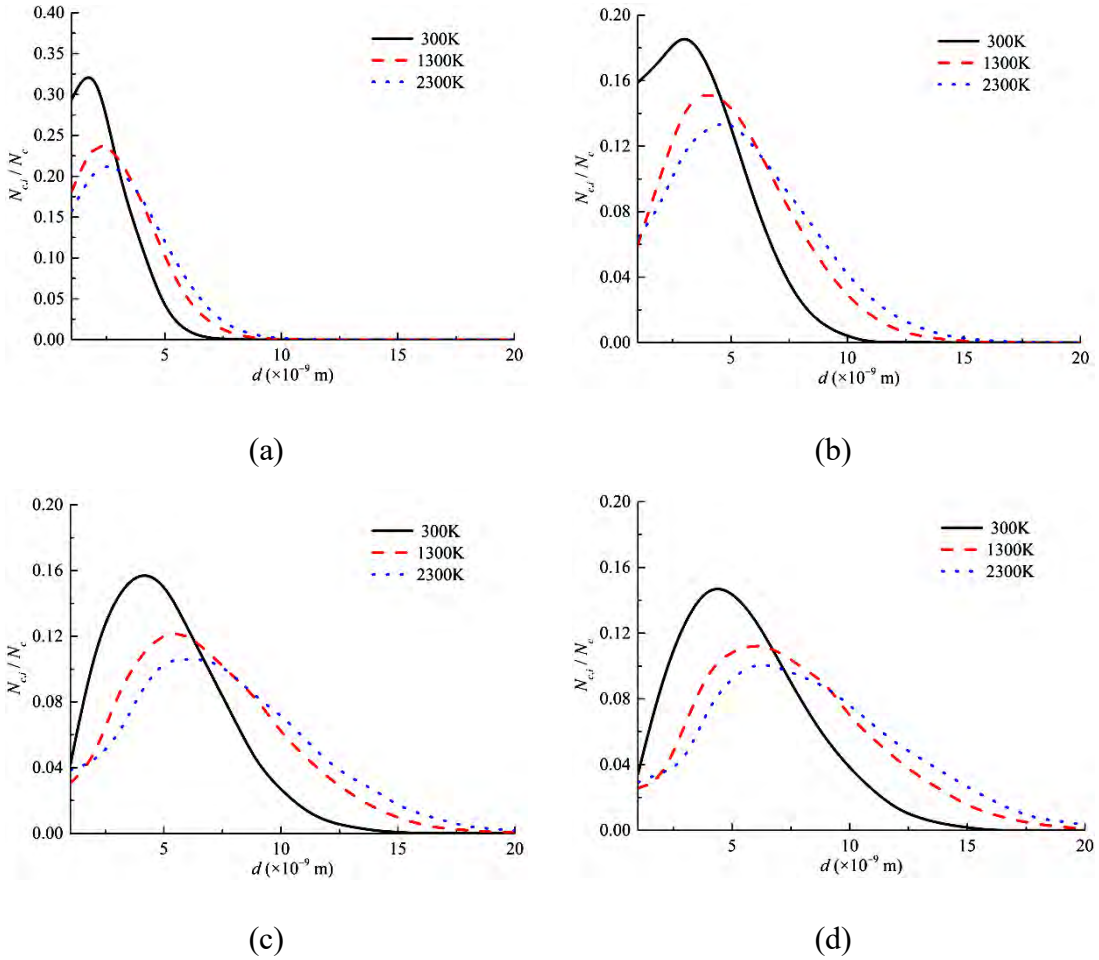

Fig. 16 PSD profiles of simultaneous coagulation and condensation cases at (a) $x/D = 2$, (b) $x/D = 6$, (c) $x/D = 10$ and (d) $x/D = 11.5$ at $y/D = 0$ and $\mathrm{Re}_D = 4000$ for different T_j.

3.3.2 The effect of Reynolds number on turbulent coagulation and condensation

Four corresponding jet Reynolds numbers, $\mathrm{Re}_D = 2000$, 4000, 6000, and 8000 are studied on two simultaneous aerosol dynamic processes (i.e., coagulation and condensation) in the turbulent planar jet for T_j =1300K. The initial conditions and Re_D are the same as previous cases studied in Section 3.2. The evolutions of the time-averaged mean particle diameters, d_{ave} and the normalized particle number concentration, $N_c/N_{c,0}$ at $y/D = 0$ of the studied cases are shown in Fig. 17.

In Fig. 17, it can be seen that for cases studied where both coagulation and condensation simultaneously occur, the mean particle diameter decreases and the particle number concentration increases with the increase of Re_D at the same jet temperature cases, because the particles have shorter time to coagulate or grow larger.

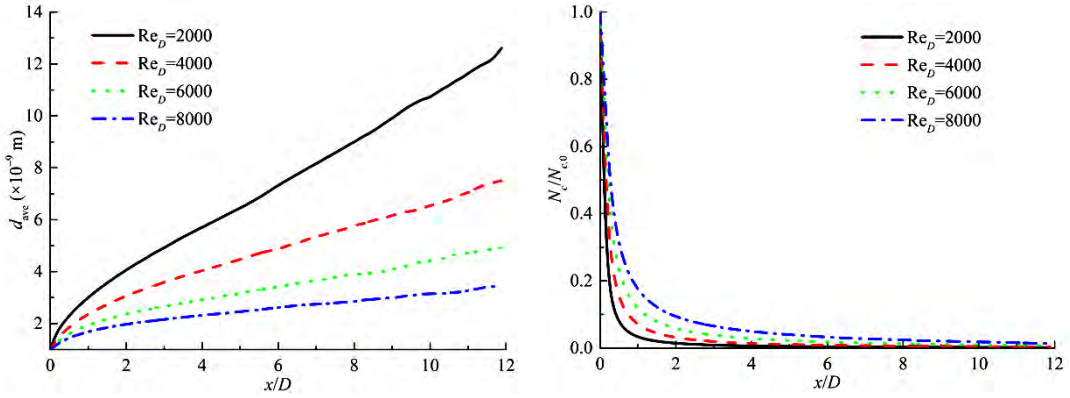

(a) (b)

Fig. 17 The spatial evolutions of the time-averaged (a) d_{ave} and (b) $N_c/N_{c,0}$ profiles at $y/D = 0$ and $T_j = 1300$K for different Re_D.

The normalized particle size distributions (PSDs) for different Re_D cases are shown in Fig. 18.

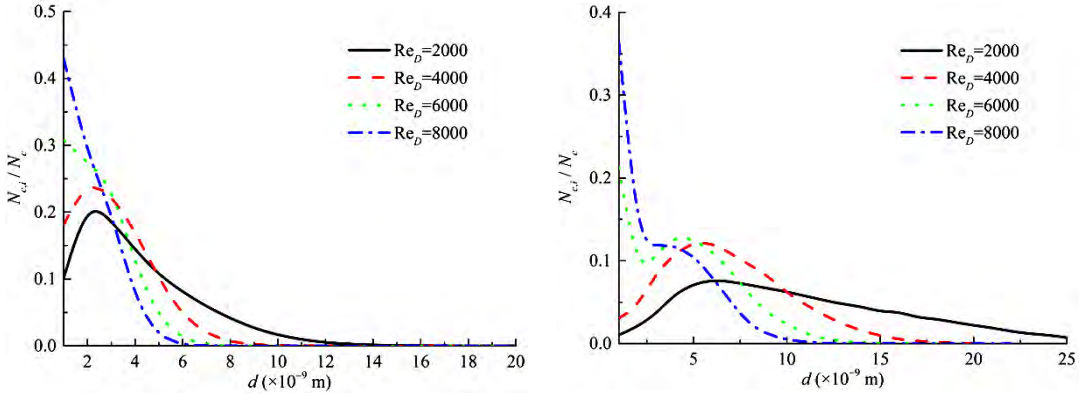

(a) (b)

Fig. 18 PSD profiles at positions of (a) $x/D = 2$, and (b) $x/D = 10$ at $y/D = 0$ and $T_j = 1300$K for different Re_D.

Similar to the cases studied when only coagulation is considered, the PSD at the same position, x/D becomes higher and narrower with the increase of Re_D when both coagulation and condensation are simultaneously considered. Therefore, when coagulation and condensation simultaneously occur, the PSD can also be controlled by adjusting Re_D accordingly.

From Fig. 18(b), with the increasing of Re_D, the evolutions of PSD at the position of x/D = 10 are basically the same with the cases studied when only coagulation is considered. When Re_D = 6000, two peaks of the PSD appeared. When Re_D = 2000, 4000 and 8000, only one peak for the PSD appeared. The reason is that coagulation becomes weaker with the increase of Re_D. When Re_D = 2000 and 4000, the coagulation effect is relatively strong, so the peak value of PSD at x/D = 10 has larger diameters; but when Re_D = 8000, the coagulation effect is relatively weak, so the peak value of PSD at x/D = 10 has a diameter of 1 nm. While Re_D=6000 is a transition value, so there are two peaks at both d = 1 nm and a larger diameter. When Re_D = 8000, the PSD also monotonically decreases. From Fig. 18, it can be concluded that the developed and coupled LES-DWOSMC method is proved to be capable of predicting the PSD when coagulation and condensation simultaneously occur in a turbulent planar jet.

3.4 Computation time analysis

The computation time of the studied cases in the present study is listed in Table 1. The normalized computation time, $\tau = t/t_0$, where t_0 is the computation time in the coagulation case used for verification. In the present study, the numerical computations are performed on 4 Intel Xeon E7-4860v2 (2.6 GHz/12 Core/30M Cache) processors with 128 GB RDIMM and the computation time in the first studied coagulation case is t_0 = 1.7 hours. From Table 2, the computation time decreases slightly with the increasing of jet temperature. This is because the particle number concentration decreases with increasing jet temperature, where less computation time is needed to calculate the particle dynamic processes. For the studied turbulent coagulation and condensation cases, the computation time is little longer than those coagulation cases because of the additional computation of condensation process. But it can also be seen that for all those cases studied, the difference of computation time among different studied cases is very small, especially between the studied cases of T_j = 1300K and 2300K, because the difference of particle number concentration between these two jet temperature cases is small, which can be seen from Figs. 10(b) and 15(b), respectively.

Table 2. Normalized computation time τ derived from different studied cases

Cases	Coagulation			Coagulation and condensation		
	T_j=300K	T_j=1300K	T_j=2300K	T_j=300K	T_j=1300K	T_j=2300K
Time τ	1	0.974	0.968	1.004	0.988	0.987

4 Conclusions

A coupled LES-DWOSMC method is newly developed to study aerosol systems in turbulent flows. The large eddy simulation (LES) method is used to compute the continuous gas flow fields and the differentially weighted operator splitting Monte Carlo (DWOSMC) method is used to simulate the simultaneous aerosol dynamic processes (i.e., coagulation and condensation processes). In this LES-DWOSMC method, both the transient particle dispersion patterns and the time-averaged properties of particles can be obtained. The evolution of time-averaged mean particle diameter, normalized particle number concentration and the particle size distribution (PSD) are observed for the studied cases. The effects of jet temperature, T_j and Reynolds number, Re_D on the evolution of particle size distribution (PSD) are fully studied.

The results show that the particle dispersion pattern is significantly affected by the vortex structure. Both coagulation and condensation processes will result in larger particle diameter and wider PSD. The high temperature will greatly enhance the coagulation rate and change the PSD in all of the studied cases. The increase of Re_D decreases the residence time of particles and results in lower occurrence of simultaneous coagulation and condensation processes, which will further affect the PSD of the particles. Re_D does not only affect the height and width of the PSD, but also affects the number of peaks of the PSD. Re_D and T_j are proved to be two important parameters that can be used to control the evolution of PSD in an aerosol reactor. The developed and coupled LES-DWOSMC method is proved to be a computationally efficient method and capable of dealing with aerosol dynamics in turbulent flows that can be very useful in many natural and engineering applications and problems.

Acknowledgements

This work was supported by the research studentship grant, the Central Research Grant (Project No. 4-BCD3 and B-Q54U) and Mechanical Engineering Department

(Project No. 88Y9) of The Hong Kong Polytechnic University, the National Natural Science Foundation of China (Project no. 11572274) and the General Research Fund, Research Grants Council of the Hong Kong Special Administrative Region, China (Project No. PolyU 152663/16E).

References

Armenio, V. and Fiorotto, V. (2013) 'The importance of the forces acting on particles in turbulent flows', *Physics of Fluids*, Vol. 13 No. 8, pp. 2437–2440.

Boyd, I. D. (1996) 'Conservative Species Weighting Scheme for the Direct Simulation Monte Carlo Method', *Journal of Thermophysics and Heat Transfer*, Vol. 10 No. 4, pp. 579–585.

Celnik, M., Patterson, R., Kraft, M. and Wagner, W. (2007) 'Coupling a stochastic soot population balance to gas-phase chemistry using operator splitting', *Combustion and Flame*, Vol. 148, pp. 158–176.

Chan, T. L., Bao, F. B., Lin, J. Z., Zhou, Y. and Chan, C. K. (2008) 'Temporal stability of a particle-laden jet', *International Journal of Multiphase Flow*, Vol. 34 No. 2, pp. 176–187.

Chan, T. L., Lin, J. Z., Zhou, K. and Chan, C. K. (2006) 'Simultaneous numerical simulation of nano and fine particle coagulation and dispersion in a round jet', *Journal of Aerosol Science*, Vol. 37 No. 11, pp. 1545–1561.

Chan, T. L., Liu, S. Y. and Liu, H. J. (2019) 'A numerical study on particle formation and evolution of a vehicular exhaust plume using the bimodal TEMOM', *Particuology,*Vol. 37 No. 43, pp. 46–55.

Chan, T. L., Liu, S. Y. and Yue, Y. (2018) 'Nanoparticle formation and growth in turbulent flows using the bimodal TEMOM', *Powder Technology*. Vol. 323, pp. 507–517.

Chan, T. L., Liu, Y. H. and Chan, C. K. (2010) 'Direct quadrature method of moments for the exhaust particle formation and evolution in the wake of the studied ground vehicle', *Journal of Aerosol Science*. Vol. 41 No. 6, pp. 553–568.

Chan, T. L., Luo, D. D., Cheung, C. S. and Chan, C. K. (2008) 'Large eddy simulation of flow structures and pollutant dispersion in the near-wake region of the studied ground vehicle for different driving conditions', *Atmospheric Environment*, Vol. 42, pp. 5317–5339.

Chen, Z., Yuan, F. and Jiang, R. J. (2015) 'Different approximate models of the sectional method for nanoparticle Brownian coagulation', *International Journal of Numerical Methods for Heat and Fluid Flow*, Vol. 25 No. 2, pp. 438–448.

Deville, R. E. L., Riemer, N. and West, M. (2011) 'Weighted Flow Algorithms (WFA) for stochastic particle coagulation', *Journal of Computational Physics*. Vol. 230 No. 23, pp. 8427–8451.

Dinneen, S. R., Deravi, L. F. and Greenslade, M. E. (2018) 'An iterative correction approach used to retrieve the refractive index of squid pigment aerosols', *Journal of Optics (United Kingdom)*. IOP Publishing, 20(3).

Eibeck, A. and Wagner, W. (2001) 'Stochastic particle approximations for Smoluchoski's coagulation equation', *The Annals of Applied Probability*, Vol. 11 No. 4, pp. 1137-1165.

Fan, J., Zhang, X., Chen, L. and Cen, K. (1997) 'New stochastic particle dispersion modeling of a turbulent particle-laden round jet', *Chemical Engineering Journal*, Vol. 66 No. 97, pp. 207–215.

Fang, J., Wang, Y., Kangasluoma, J., Attoui, M., Junninen, H., Kulmala, M., Petäjä, T. and Biswas, P. (2018) 'The initial stages of multicomponent particle formation during the gas phase combustion synthesis of mixed SiO2/TiO2', *Aerosol Science and Technology*. Taylor & Francis, Vol. 52 No. 3, pp. 277–286.

Friedlander, S. K. (2000) *Smoke, dust and haze: fundamentals of aerosol*. New York: Oxford University Press.

Kruis, F. E., Wei, J., Zwaag, T., and Haep, S. (2012). 'Computational fluid dynamics based stochastic aerosol modeling: Combination of a cell-based weighted random walk method and a constant-number Monte-Carlo method for aerosol dynamics'. *Chemical Engineering Science*, Vol. 70, pp. 109–120.

Kotalczyk and G., Kruis, F.E. (2017) 'A Monte Carlo method for the simulation of coagulation and nucleation based on weighted particles and the concepts of stochastic resolution and merging'. *Journal of Computational Physics*, Vol. 340, pp. 276–296.

Kotalczyk and G., Kruis, F.E. (2018) 'Fractional Monte Carlo time steps for the simulation of coagulation for parallelized flowsheet simulations'. *Chemical Engineering Research and Design*, Vol. 136, pp. 71–82.

Köhn, C., Enghoff, M. B., and Svensmark, H. (2018) 'A 3D particle Monte Carlo approach to studying nucleation', *Journal of Computational Physics*, Vol. 363, pp. 30–38.

Lee, K. F., Patterson, R. I. A., Wagner, W. and Kraft, M. (2015). 'Stochastic weighted particle methods for population balance equations with coagulation, fragmentation and spatial inhomogeneity', *Journal of Computational Physics*, Vol. 303 No.19, pp.1-18.

Lin, J. Z., Chan, T. L., Liu, S., Zhou, K., Zhou, Y. and Lee, S. C. (2007) 'Effects of coherent structures on nanoparticle coagulation and dispersion in a round jet', *International Journal of Nonlinear Sciences and Numerical Simulation*, Vol. 8 No. 1, pp. 45–54.

Liu, H. M. and Chan, T. L. (2016) 'A new differentially weighted operator splitting Monte Carlo method for aerosol dynamics.', in *Proceedings of the 24th International Conference on Modelling, Monitoring and Management of Air Pollution (Air Pollution 2016), June 20-22, 2016, Crete, Greece.*, pp. 237–248.

Liu, H. M. and Chan, T. L. (2018a) 'Differentially weighted operator splitting Monte Carlo method for simulating complex aerosol dynamic processes', *Particuology*, Vol. 36, pp. 114–126.

Liu, H. M. and Chan, T. L. (2018b) 'Two-component aerosol dynamic simulation using differentially weighted operator splitting Monte Carlo method', *Applied Mathematical Modelling*. Vol. 62, pp. 237–253.

Liu, S. Y. and Chan, T. L. (2017a) ‘A coupled CFD-Monte Carlo method for simulating complex aerosol dynamics in turbulent flows’, *Aerosol Science and Technology*. Vol. 51 No. 3, pp. 269–281.

Liu, S. Y. and Chan, T. L. (2017b) ‘A stochastically weighted operator splitting Monte Carlo (SWOSMC) method for the numerical simulation of complex aerosol dynamic processes’, *International Journal of Numerical Methods for Heat and Fluid Flow*, Vol. 27, pp. 263–278.

Liu, S. Y., Chan T. L., He Z., Lu Y. Y., Jiang X. and Wei F. Z. (2019) ‘Soot formation and evolution characteristics in premixed methane/ethylene-oxygen-argon burner-stabilized stagnation flames’. *Fuel*, Vol. 242, pp. 871-882.

McLachlan, R., Quispel, G., (2002) 'Splitting methods', *Acta Numerica*, pp. 341–344.

McGraw, R. (1997) ‘Description of aerosol dynamics by the quadrature method of moments’, *Aerosol Science and Technology*, Vol. 27 No. 2, pp. 255–265.

Miller, S. E. and Garrick, S. C. (2004) ‘Nanoparticle coagulation in a planar jet’, *Aerosol Science and Technology*, Vol. 38 No. 1, pp. 79–89.

Patterson, R. I. A., Wagner, W. and Kraft, M. (2011) 'Stochastic weighted particle methods for population balance equations', *Journal of Computational Physics*, Vol. 230 No.19, pp.7456-7472.

Pesmazoglou, I. Kempf, A. M. and Navarro-martinez, S. (2017) ‘Large eddy simulation of particle aggregation in turbulent jets’, *Journal of Aerosol Science*. Vol. 111, pp. 1–17.

Pesmazoglou, I., Kempf, A. M. and Navarro-martinez, S. (2016) ‘Stochastic modelling of particle aggregation’, *International Journal of Multiphase Flow*. Vol. 80, pp. 118–130.

Prakash, A., Bapat, A. P. and Zachariah, M. R. (2003) ‘A simple numerical algorithm and software for solution of nucleation, surface growth, and coagulation problems’, *Aerosol Science and Technology*, Vol. 37 No. 11, pp. 892–898.

Ramabhadran, T. E., Peterson, T. W. and Seinfeld, J. H. (1976) ‘Dynamics of aerosol coagulation and condensation’, *AIChE Journal*, Vol. 22 No. 5, pp. 840–851.

Rigopoulos, S. (2007) ‘PDF method for population balance in turbulent reactive flow’, *Chemical Engineering Science*, Vol. 62, pp. 6865–6878.

Rjasanow, S. and Wagner, W. (1996) ‘A stochastic weighted particle method for the Boltzmann equation’, *Journal of Computational Physics*, Vol. 124 No. 2, pp. 243–253.

Rodrigues, P., Franzelli, B., Vicquelin, R., Gicquel, O. and Darabiha, N. (2018) ‘Coupling an LES approach and a soot sectional model for the study of sooting turbulent non-premixed flames’, *Combustion and Flame*. Vol. 190, pp. 477–499.

Smagorinsky, J. (1963) ‘General circulation experiments with the primitive equations’, *Monthly Weather Review*, Vol. 91 No. 3, pp. 99–164.

Smith, M. and Matsoukas, T. (1998) ‘Constant-number Monte Carlo simulation of population balances’, *Chemical Engineering Science*, Vol. 53 No. 9, pp. 1777–1786.

Sommerfeld, M. (2001) ‘Validation of a stochastic Lagrangian modelling approach for inter-particle collisions in homogeneous isotropic turbulence’, *International Journal of Multiphase Flow*, Vol. 27, pp. 1829–1858.

Stark, W. J. and Pratsinis, S. E. (2002) ‘Aerosol flame reactors for manufacture of nanoparticles’, *Powder Technology*, Vol. 126, pp. 103–108.

Sung, Y., Raman, V. and Fox, R. O. (2011) ‘Large-eddy-simulation-based multiscale modeling of TiO2 nanoparticle synthesis in a turbulent flame reactor using detailed nucleation chemistry’, *Chemical Engineering Science*. Elsevier, Vol. 66 No. 19, pp. 4370–4381.

Wei, J. (2013) ‘A fast monte carlo method based on an acceptance-rejection scheme for particle coagulation’, *Aerosol and Air Quality Research*, Vol. 13 No. 4, pp. 1273–1281.

Yu, M., Lin, J. and Chan, T. (2008) ‘Numerical simulation of nanoparticle synthesis in diffusion flame reactor’, *Powder Technology*, Vol. 181, pp. 9–20.

Zhao, H., Kruis, F. E. and Zheng, C. (2010) ‘A differentially weighted Monte Carlo method for two-component coagulation’, *Journal of Computational Physics*, Vol. 229 No. 19, pp. 6931–6945.

Zhao, H. and Zheng, C. (2013) ‘A population balance-Monte Carlo method for particle coagulation in spatially inhomogeneous systems’, *Computers & Fluids*, Vol. 71, pp. 196–207.

Zhao, H., Zheng, C. and Xu, M. (2005) ‘Multi-Monte Carlo method for coagulation and condensation/evaporation in dispersed systems’, *Journal of Colloid and Interface Science*, Vol. 286 No. 1, pp. 195–208.

Zhou, K. and Chan, T. L. (2011) ‘Simulation of homogeneous particle nucleation in a free turbulent jet’, *Aerosol Science and Technology*, Vol. 45 No. 8, pp. 973–987.

Zhou, K. and He, Z. (2014) ‘Monte Carlo simulation of aerosol evolution in a planar mixing layer’, *International Journal of Numerical Methods for Heat and Fluid Flow*, Vol. 24 No. 8, pp. 1769–1781.

Zhou, K., He, Z., Xiao, M., Zhang, Z., (2014) ‘Parallel Monte Carlo simulation of aerosol dynamics’, *Advances in Mechanical Engineering* , Vol. 6, pp. 1–11.